Fe_2O_3-TiO_2 Core-Shell Nanorod Arrays for Visible Light Photocatalytic Applications

Kun Yao,[1,2] Pradip Basnet,[2,3] Henry Sessions,[4] George K. Larsen,[4]
Simona E. Hunyadi Murph,[4,5*] and Yiping Zhao[2,3*]

[1] *College of Engineering, University of Georgia, Athens, GA, 30602, USA*

[2] *Nanoscale Science and Engineering Center, University of Georgia, Athens, GA, 30602, USA*

[3] *Department of Physics and Astronomy, University of Georgia, Athens, GA, 30602, USA*

[4] *National Security Directorate, Savannah River National Laboratory, Aiken, SC, USA*

[5] *Chemistry and Physics Department, Georgia Regents University, Augusta, GA, USA*

**Corresponding authors- Email address: Simona.Murph@srnl.doe.gov, Phone: 1-803-646-676,*
Email address: zhaoy@physast.uga.edu, Phone: 1-706-542-7792.

Abstract

By using the glancing angle deposition technique and post-deposition annealing, Fe_2O_3-TiO_2 core-shell nanorod arrays with specific crystalline states can be designed and fabricated. The Fe_2O_3-TiO_2 core-shell samples annealed at temperatures greater than 450°C formed α-Fe_2O_3 and anatase TiO_2, and showed higher catalytic efficiency for the degradation of methylene blue (MB) under visible light illumination when compared with pure anatase TiO_2 or α-Fe_2O_3 nanorod arrays. Solar conversion of carbon dioxide and water vapor in the presence of Fe_2O_3-TiO_2 core-shell nanorod arrays was also investigated. Carbon monoxide, hydrogen, methane, and methanol along with other hydrocarbons were produced after only several hours' exposure under ambient sunlight. It was determined that the core-shell structure showed greater efficiency for solar CO_2 conversion than the pure TiO_2 nanorod arrays.

Keywords: Glancing angle deposition; nanorod arrays; core-shell Fe_2O_3-TiO_2.

1. **Introduction**

In recent years, researchers have spent considerable effort in developing methods to use solar energy more efficiently in order to achieve a sustainable solution to the world's long term energy crisis. One promising strategy is to design and fabricate highly efficient photocatalysts that use solar illumination to facilitate chemical reactions that produce a fuel, reduce pollution, or both [1-3]. Among the materials studied and proposed, metal oxides nanostructures have attracted the most attention as photocatalysts due to their large surface-to-volume ratio, adjustable band gap E_g, and superior stability [4-8]. Particularly, TiO_2 photocatalysts have been investigated extensively for solar water splitting, CO_2 conversion, environmental decontamination, among others [9-11]. Its non-toxicity, low cost, and high stability make TiO_2 suitable for those applications. However, the large E_g value of TiO_2 ($E_g = 3.2$ eV) inhibits the absorption of the visible light, the largest part of the solar spectrum, which significantly limits the solar conversion efficiency. Therefore, in order to efficiently utilize most of the solar spectrum, current research has focused on designing novel complex nanostructures with a broad wavelength range for light absorption in the UV-Vis-near infrared region [12-16]. There are two common approaches to increasing the visible light absorption of TiO_2: coupling with a lower band gap material (Fe_2O_3, Cu_2O, CuO, CdSe, CdTe, etc.) to create a semiconductor junction [3, 17, 18] or doping or co-doping with non-metals (carbon, sulfur, fluorine, nitrogen, etc.) [6, 19] and metals (silver, gold, platinum, etc.) [20]. Among these two approaches, coupling TiO_2 with smaller band gap semiconductors has distinct advantages: the band gap can easily tuned by selecting different semiconducting materials, the semiconductor junction can spatially separate electron-hole pairs and thereby decrease recombination rates, and finally, combining two or more semiconductors is a relatively simple process that is compatible with many different fabrication techniques.

Hematite, α-Fe_2O_3, is an active nanocatalyst material that makes an interesting companion to TiO_2 due to its narrow band gap (E_g = 2.2 eV), low cost, and high stability. Recent studies show that TiO_2-Fe_2O_3 multi-layered thin films and other composite structures (*e.g.*, α-Fe_2O_3 particles coated TiO_2 nanosheets, core–shell structured TiO_2-Fe_2O_3 nanocomposites) are active in the UV-visible region of the spectrum and can be more efficient photocatalysts than pure TiO_2 toward degradation of a variety of organic compounds [7, 21-26]. The higher catalytic efficiency results from greater visible light absorption, and enhanced charge separation of the electron-hole pairs. Particularly, under visible light, electron-hole pairs only generate in Fe_2O_3 but not in TiO_2. Thus electrons could be transferred from to conduction band of Fe_2O_3 to TiO_2, while the holes remain in the valence band of Fe_2O_3 [22, 24, 26-28]. The nature of the contact between TiO_2 and Fe_2O_3 is also critical in determining the efficiency of the charge separation process and overall catalytic efficiency. Recently, it was reported that the enhanced photocatalysis of Fe_2O_3-TiO_2 nanocomposites is mainly due to the junction or co-catalyst effect for reactions [3]. There are also a number of other factors that affect the photocatalytic processes, including the surface area, nanoparticle's size and shape, crystallinity, electron-hole recombination rate, heterojunction and synergistic effects between materials, as well as adsorbent - adsorbate interaction [22, 24, 26-28].

Therefore, it is interesting to explore new architectures and fabrication techniques in order to further study and optimize the TiO_2-Fe_2O_3 system for highly efficient photocatalysts.

Glancing angle deposition (GLAD) is a simple and well-known technique in which the incident material vapor is directed toward a substrate at large incident angles with respect to substrate surface normal (> 70°), while the substrate is rotated azimuthally at a constant speed, resulting in self-organized vertically align nanorod arrays [13, 29-31]. Our previous work has proven that this is a versatile method in fabricating TiO_2-WO_3 core-shell structured photocatalysts [13, 32]. Additionally, the dynamic shadowing growth (DSG) technique has several advantages for metal oxide nanostructure fabrication: simplicity, flexibility, and compatibility with other microfabrication techniques.

In this work, we design and fabricate Fe_2O_3-TiO_2 core-shell nanorod arrays using the GLAD technique. The core-shell architecture is chosen to maximize the interfacial contact between Fe_2O_3 and TiO_2 and is expected to increase charge separation and catalytic efficiency. A post-deposition annealing treatment is developed in order to obtain a structure with twofold active crystalline phases, α-Fe_2O_3 and anatase TiO_2. In addition to their morphological, structural, and optical properties, the visible light photocatalytic activities of the Fe_2O_3-TiO_2 core-shell samples for methylene blue destruction and CO_2 conversion are investigated. It is found that the α-Fe_2O_3-TiO_2 core-shell nanorods arrays are more efficient photocatalysts for both of these processes under visible light illumination than either of the pure material photocatalysts, TiO_2 and Fe_2O_3.

2. Materials and methods

The source materials used in this study, Fe_2O_3 (99.85+%, metal base), and TiO_2 (99.9 %) were purchased from Alfa Aesar (Ward Hill, MA) and Kurt J. Lesker (Clairton, PA), respectively and were used as received. Cleaned glass microscope slides (Gold Seal ® Catalog No. 3010) and Si (100) wafers (Montco Silicon Technologies Inc.) were used as substrates for material deposition. High purity methylene blue (MB, C16H18ClN3S; CAS #122965-43-9) was obtained from Alfa-Aesar (Ward Hill, MA).

2.1. Fe_2O_3-TiO_2 core-shell nanorod arrays preparation

The nanorod arrays were fabricated in a custom designed electron-beam deposition system (Torr International, Inc.) [13, 33]. Fe_2O_3 nanorods was first deposited onto Si and/or glass substrates with the incident angle $\theta = 86^{\circ}$, with the substrate rotating azimuthally at 0.5 rev/s. The deposition proceeded until a nominal thickness of 3 um, as determined by a quartz crystal microbalance (QCM), was achieved. Based on the nanorod separation and height measured using scanning electron microscopy, the vapor incident angle for the TiO_2 shell deposition was determined to be $\theta = 6.1^{\circ}$. Further details describing this calculation and the GLAD core-shell deposition method can be found in Ref [13]. Using the same substrate azimuthal rotation rate of 0.5 rev/s, the TiO_2 shell was deposited to a nominal thickness of 50 nm. The as-deposited Fe_2O_3-TiO_2 nanorod samples were then annealed in a quartz tube furnace (Lindberg/ Blue M Company) in open air for 3 hours, at different preset temperatures from 350 °C to 750 °C.

2.2 Characterization

The morphologies of the samples were examined by a field-emission scanning electron microscope (SEM, FEI Inspect F) equipped with an energy dispersive X-ray spectrometer (EDX). The structural properties of the samples were characterized by a PANalytical X'Pert PRO MRD X-ray diffractometer (XRD) with fixed incidence angle of 1.5°. The XRD patterns were recorded with Cu Kα radiation ($\lambda = 1.5405980$ Å) in the 2θ range from 20°-80° at step size of 0.014°. The optical properties of the samples were measured by a double beam UV-visible light (UV-vis) spectrophotometer (JASCO V-570) over a wavelength range from 300 to 800 nm. The photocatalytic activities of the samples were evaluated by the photocatalytic degradation of a 10 ppm (~31 μM) methylene blue (MB) aqueous solution (of pH value ~6.2) under visible light irradiation. The TiO_2, Fe_2O_3, or Fe_2O_3-TiO_2 samples on glass substrates were placed into a 10 mm × 10 mm × 45 mm clear methacrylate cuvette filled with 4.0 ml of MB solution. The cuvettes were illuminated for a total time of 4 hours by a 250 W quartz halogen lamp (UtiliTech) covering wavelength range from 400 to 800 nm. The incident light intensity on sample was kept constant at 65 mW/cm^2, as measured by an optical power meter (Thorlabs PM100D/S310C). A rectangular mask (2.4 cm^2) was placed in front of the all samples to keep the light power the same for all photodegradation experiments. A water filter was placed in front of the cuvette to absorb the IR light. The photodegradation the MB solution were measured by examining the in-situ UV-Vis transmission spectra of the MB solution using an Ocean Optics spectrophotometer (USB 2000). The absorbance peak at $\lambda = 664$ nm was monitored at regular time increments of 20 min and were used to evaluate the photodegradation rate of MB. For the CO_2 photoconversion study, a syringe-type chamber (volume of 20 ml) was designed as solar-gas convertor reactor with gas inlets/outlets, optical window and sample stage holder. It was loaded with three 1x1 cm^2 Fe_2O_3-TiO_2 core-shell nanorod array samples (or control samples of TiO_2 nanorod arrays) in CO_2 and H_2O gas mixture in ambient light and atmospheric conditions. The evolving gas in this system was probed by micro gas-chromatograph (GC) instrumentation equipped with OV1 and pora-plot columns.

3. Results and Discussion

3.1 Morphology and composition of the core-shell structures

The Fe_2O_3 nanorod samples, which serve as the "core" template in the core-shell structure, were analyzed using scanning electron microscopy (SEM). As shown in Figure 1a, the arrays consist of well separated and vertically aligned nanorods with tetrahedral facets. The overall array morphology is consistent with GLAD growth. The morphologies of the individual nanorods is consistent with a fiber texture resulting from a preferred growth direction, where the exposed facets are the low energy crystalline planes, most likely [34, 35]. Quantitative measurements of the SEM images reveal that the average height of the Fe_2O_3 nanorods is h = 1220 ± 30 nm, and the diameter at the top is D_T = 230 ± 50 nm. The average nanorod separation (edge-to-edge distance of two adjacent nanorods) is d = 130 ± 40 nm, and the nanorod density is $\eta = 10\ \mu m^{-2}$. Figure 1b shows the top view and the cross-sectional SEM images of the core-shell Fe_2O_3-TiO_2 nanorod array. In comparing the nanorod arrays before and after deposition of TiO_2 (Figures 1a and 1b, respectively), it can be observed that the TiO_2 coating creates a thin, porous shell over the Fe_2O_3 nanorod surface. High resolution transmission electron microscopy (TEM) imaging was performed to further investigate the morphology of the individual nanorods. Figure 2 shows TEM micrographs of as-deposited and 500 °C annealed Fe_2O_3-TiO_2 core-shell nanorods. As can be seen in the images, the TiO_2 coating appears as a ~50 nm porous layer surrounding the Fe_2O_3 core, giving the whole structure a feather-like appearance. The feather-like appearance of the TiO_2 shell (indicated by the arrows) is consistent with previous reports reported by our group [32]. Lattice fringes can be seen in the porous TiO_2 structures after annealing, and the spacing 0.36 nm agrees well with the (101) lattice plane of anatase TiO_2.

Table I summarizes the measured parameters of the nanorod array before and after TiO_2 shell deposition. As expected, when compared with the Fe_2O_3 core, the core-shell nanorods become longer and wider after the TiO_2 shell deposition, where the core-shell Fe_2O_3-TiO_2 nanorod have h = 1230 ± 30 nm, D_T = 240 ± 40 nm and d = 110 ± 60 nm. The nanorod density, η, remains unchanged after the shell deposition, which indicates that the deposition primarily occurs on the original Fe_2O_3 core structure. Finally, the EDX spectra confirm the presence of a TiO_2 layer

(Figures 3a and 3b) in showing a Ti peak and an increase in the O peak intensity after the shell deposition.

3.2. Optimizing annealing condition

Previous studies indicate that anatase TiO_2 and α-Fe_2O_3 have a higher photocatalytic efficiency than the amorphous structure or other crystal phases of TiO_2 and Fe_2O_3 [22]. Thus, various annealing treatments were performed in order to obtain these phases and, subsequently, the most efficient catalytic response. Figure 4 shows the XRD results of the core-shell samples annealed at different temperatures. The spectrum of the as-deposited sample shows only the diffraction peak from the (110) plane of α-Fe_2O_3 at $2\theta = 35.4°$, which suggests preferential growth along the [110] direction and is consistent with previous results [36]. After annealing at 350°C, an additional peak at $2\theta = 25.3°$ emerges and is attributed to the (101) plane of anatase TiO_2. At 450 °C, additional peaks from α-Fe_2O_3 are observed, but the relative intensity of the (104) plane is greater than the (110) plane, indicating that the amorphous to crystalline transition exhibits no preferential growth direction. The diffraction pattern at 550°C is similar to the one at 450°C. However, once the annealing temperature is increased to 650°C, the α-Fe_2O_3 diffraction peak intensities begin to decrease, which could be due to alloying of Fe-Ti-O. Finally, at 750°C, most α-Fe_2O_3 peaks have disappeared. These results demonstrate that the optimal annealing temperature for the Fe_2O_3-TiO_2 core-shell nanorod arrays is between 450°C and 550°C. It is important to note that, in general, the α-Fe_2O_3 diffraction peaks are more pronounced than the anatase TiO_2 crystal peaks because the amount of Fe_2O_3 is greater than the amount of TiO_2 in the core-shell samples.

3.3 Optical property

The optical properties were investigated for the as-prepared Fe_2O_3-TiO_2 samples and the samples annealed at 350°C, 450°C and 550°C since these showed no evidence of alloying. Figures 5a and 5b show the transmission spectra $T(\lambda)$ and the absorption spectra extracted from $T(\lambda)$, respectively. To simplify the analysis, we assume that extinction = absorption + scattering, where the scattering by the samples is assumed to be independent of wavelength over the measured region [37]. In this assumption, the wavelength dependence of extinction is in proportion to $\alpha(\lambda)$, and can be calculated from Beer–Lambert law $\alpha(\lambda) = 1/d \ln(1/T)$, where d indicates the thickness of the sample.

The as-prepared and the 350°C annealed samples show similar transmission and absorption spectra, with the rising edge of around 600 nm, implying that amorphous or α-Fe_2O_3 are the dominant forms present in our sample [38, 39]. However, the samples annealed at 450°C and 550°C show greatly decreased transmission and enhanced absorption in the visible light range. As discussed above, these annealing temperatures induced an amorphous to polycrystalline α-Fe_2O_3 transition in the core-shell nanorods, and therefore, this increase in absorption over the visible range is attributed to formation of α-Fe_2O_3. It is expected that the significant visible light absorption, coupled with the active hematite and anatase phases, should make the samples annealed at 450°C and 550°C efficient visible light photocatalysts.

In designing core-shell photocatalysts, it is important to consider the optical properties of the individual materials. In particular, it is important that TiO_2 “shell” reside on the Fe_2O_3 “core” as the outside-shell layer. Such a design results in an efficient utilization of both core and shell layers because the visible light can pass through and get absorbed by the Fe_2O_3 core. Otherwise, if the core-shell materials are switched and the narrower band gap material Fe_2O_3 serves as the shell layer, it will adsorb both visible light and UV light and inhibit the light absorption in the TiO_2 core layer, reducing photocarrier generation [13].

3.4. Photodegradation of MB aqueous solution

In order to elucidate the photocatalytic behavior of the Fe_2O_3-TiO_2 core-shell nanorod arrays, both UV and visible light photodegradation experiments were performed. Methylene blue (MB) dye is selected as the probe molecule for photodegradation because it is widely used to represent wastewater contamination [32, 40, 41]. Figure 6a shows the spectra of the UV lamp (center wavelength of 365 nm) and the white lamp (broadband over 350 nm to 900 nm) used for the MB degradation study. Prior to the photodegradation experiments, two control experiments were performed. The first control experiment monitored Fe_2O_3-TiO_2 core-shell nanorod arrays placed in dye solutions that were kept in the dark for 30 to 60 min. This dark experiment resulted in very little degradation of the dye (Figure 6c). The second control experiment investigated the direct photodegradation of the dyes by illuminating solutions in the absence of a photocatalyst. Some decay is noted, with a rate constant of $k = 0.003 \pm 0.001$ hr^{-1} (this calculation is discussed in greater detail below). This relatively slow decrease in absorption spectra of MB solution (note that y-axis is in negative log) suggests that there is a small amount of self-degradation of MB under visible light irradiation.

After performing the control experiments, the photocatalytic activity of the Fe_2O_3-TiO_2 samples were evaluated by monitoring the change in the absorbance of a MB aqueous solution as a function of photocatalyst irradiation time. The time evolution of the MB absorbance peak at $\lambda \approx$ 664 nm is used to calculate the decay rate k. Figure 6b shows representative absorbance curves of the MB solution using a 450°C annealed sample as the photocatalyst under visible light illumination. The absorbance of the solution is clearly decreasing, indicating the continuous degradation of MB. In order to quantify and compare the decay rates of the different samples, we assume that photodegradation exhibits first-order reaction kinetics. Thus, one can assume the following: $\alpha(t) = \alpha(0)\ e^{-kt}$, where $\alpha(0)$ is the initial MB absorbance, $\alpha(t)$ is the MB absorbance at time t, and k is the rate constant. Figure 6c plots the curves of $-\ln(\alpha(t)/\alpha(0))$ versus time for the different core-shell samples under visible light illumination. The k values are extracted from the slopes of these curves and are plotted in Figure 6d. In general, the annealed nanorod array samples show higher photocatalytic capability than the as-deposited samples. Among the samples tested, the samples annealed at 450°C and 550°C present the highest decay rate, which indicates that anatase TiO_2 and α-Fe_2O_3 phases in the core-shell structure show the best catalytic effect toward MB degradation under visible light illumination, as expected.

It is also interesting to compare the effect of different illumination conditions on the photocatalytic activity of the core-shell samples. Thus, figure 6d also shows the calculated decay rate k for the different samples when illuminated with both visible and UV light at the same time. For all samples, the value of k is higher when using both UV and visible light. This could be attributed to the fact that both UV and visible light are used to activate the individual materials. That is, UV light excites electron-hole pairs in TiO_2 and visible light excites electron-hole pairs in Fe_2O_3, and the presence of both carriers in both materials may facilitate charge transfer by decreasing recombination rates. As a corollary, when the photodegradation is performed using only UV light, the Fe_2O_3-TiO_2 core-shell nanorod samples show relatively low photocatalytic activity (Table II). This could be related to the Fe^{3+} ions in Fe_2O_3, as these have been reported to act as recombination centers for the photogenerated electrons and holes of TiO_2 [26]. It is also worthwhile to note that the mechanism of dye degradation with UV and visible light could proceed through different mechanisms due to the possibility of dye sensitization, *i.e.*, electron transfer from the photoexcited dye to the photocatalyst under visible light irradiation [37]. Other studies suggests that, at the interface of coupled Fe_2O_3 and TiO_2 heterojunction, the Fermi level of Fe_2O_3 and TiO_2 is aligned in equilibrium [22, 24, 27]. As a result, the photogenerated electrons under visible light illumination can transfer from CB of Fe2O3 to that of TiO_2 driven by the action of built-in electric field and the concentration gradient, while the holes accumulate in VB of Fe_2O_3 due to the lower voltage forbidden. Through this separation progress, the recombination of photogenerated electrons and holes is inhibited to a certain extent. The electrons in CB of TiO_2 will react with O_2 species and form the superoxide anion O_2^- and hydroxyl radicals (•OH). The accumulated holes in VB of Fe_2O_3 will further react with hydroxyl ions OH^- to produce reactive radicals, such as $•O_2$ and •OH. The resultant •OH radicals will further decompose the organic analytes effectively as a powerful oxidant. The interface between Fe_2O_3 and TiO_2 is also critical for determining the photocatalytic properties of these structures. [28]. Therefore, it is possible that the observed higher degradation rates could result from the combination of dye sensitization and charge generation from within the photocatalyst. In any case, the Fe_2O_3-TiO_2 core-shell nanorod are efficient photocatalysts with a maximum decay rate of $k = 0.151 \pm 0.001$ h^{-1}, under visible light illumination. In comparison, this is about 3.5 times higher than Ag-embedded TiO_2 nanorods investigated in our previous work [37].

Finally, it is important to determine the effectiveness of the core-shell structure when compared to the single material structure. Thus, pure α-Fe_2O_3 and anatase TiO_2 nanorod arrays of identical geometry and dimensions were also synthesized and investigated as photocatalysts toward MB degradation. Their corresponding decay rates under UV or visible light are summarized in Table II. Under UV light illumination, the highest decay rate k was in the presence of TiO_2 catalyst, which is in agreement to other catalytic studies with TiO_2. However, when exposed under visible light, the core-shell sample shows the highest *k* value when compared with pure Fe_2O_3 or TiO_2. This clearly shows the effectiveness of the core-shell design versus the individual TiO_2 or Fe_2O_3 catalyst.

3.4. Solar conversion of CO_2 and H_2O vapor

Conversion of solar energy and waste chemicals, such as CO_2, into stored chemical energy, such as hydrocarbons, is arguably one of the most promising and environmentally friendly technologies for energy generation. A small fraction of the solar energy, if converted and stored, can significantly address the world's increasing energy needs and reduce reliance on fossil fuels and, hence, enhance America's energy security. As an added benefit, this conversion process utilizes the greenhouse gas CO_2 as a reactant making the process nearly (minus materials transport and catalyst manufacturing) CO_2 neutral.

The CO_2 conversion is a complex and multistep process, and the product selectivity is highly dependent on catalyst materials. Yu et al demonstrated that CO_2 can be reduced to CO and O_2 using Pt/TiO_2 catalysts [42]. Varghese et al. hypothesized that the photocatalytic reduction of CO_2 by Cu or Pt TiO_2 catalysts follows the following processes [12]:

$$CO_2 + 2e^- + 2H+ \rightarrow CO + \tfrac{1}{2} O_2 \quad (1)$$

$$H_2O + 2h^+ \rightarrow \tfrac{1}{2} O_2 + 2H^+ \quad (2)$$

$$CO_2\ (aq.) + 2H+ + 2e^- \rightarrow HCOOH \quad (3)$$

$$HCOOH + 2H+ + 2e^- \rightarrow HCHO + H_2O \quad (4)$$

$$HCHO + 2H+ + 2e^- \rightarrow CH_3OH \quad (5)$$

$$CH_3OH + 2H+ + 2e^- \rightarrow CH_4 + H2O \quad (6)$$

To investigate the photocatalytic capabilities of Fe_2O_3-TiO_2 core-shell nanorod array photocatalysts toward conversion of CO_2 and H_2O vapor mixture to fuel in our study, the optimized Fe_2O_3-TiO_2 core-shell nanorod arrays were tested in a solar-gas convertor reactor. The photoconversion was evaluated by exposing three 1x1 cm^2 Fe_2O_3-TiO_2 core-shell nanorod array samples to a CO_2 and H_2O gas mixture in ambient light and atmospheric conditions. TiO_2 nanorod array samples with the same size were also tested for comparison purpose. The chamber was a sealed syringe-type chamber (volume of 20 ml) with gas inlets/outlets, optical window and sample stage holder (SI- Figure 1). The syringe-type chamber was strategically selected for (a) admitting solar radiation under outdoor sunlight and (b) allowing a direct gas analysis with the micro gas-chromatograph without the need of intermediary sampling steps. After loading the chamber with the samples, the solar chamber was flushed for five minutes with ultra-pure Ar. CO_2 was passed through a bubbler containing deionized water, and then the CO_2 and H_2O gas mixture flowed through the chamber and equilibrated for approximately 10 min before sealing the chamber. After loading, the syringe-type chamber was sealed and exposed outside (Aiken, SC, USA) to "real atmospheric conditions".

Gas detection was achieved by micro gas-chromatograph (GC) instrumentation equipped with OV1 and pora-plot columns. Approximately, 1 ml gases were manually injected each time using the gas-tight syringe-type chamber. The photocatalysis experiments with the active catalysts were repeated three times under the similar atmospheric conditions. For calibration purpose, H_2, CO, CH_3OH and CH_4 gases (which are the most possible products) were first analyzed on the micro-GC to determine gas elution time. OV1 column was used to monitor CH_3OH, while the pora-plot column was used to detect all the other gases: H_2, CO and CH_4. Gas production was expressed as abundance and was determined by evaluating the area peak of the gas eluted on the micro-GC instrumentation. It is worth mentioning that all of the product gases of interests, *e.g.* H_2, CO, CH_3OH, CH_4, etc., are only detected in the presence of the photocatalysts. Figure 7a compares the production of H_2 and CO in the presence of Fe_2O_3-TiO_2 core-shell or TiO2 nanorod array photocatalysts after exposure for 4 hours. The amount of H_2 produced is three times higher in the presence of Fe_2O_3-TiO_2 core-shell nanorod arrays than TiO_2 nanorod arrays. The amount of CO produced in the presence of Fe_2O_3-TiO_2 core-shell samples is also higher than TiO_2 nanorod. These results are in good agreement with the MB absorption spectra and photodegradation results shown in Figure 5 and Figure 6, respectively, due to the coupling of TiO_2 with Fe_2O_3 which extends the adsorption of solar energy in visible region and generates more electron-hole pairs.

Figure 7b shows the monotonic increase of H_2 evolution after exposure for 0, 4 and 16 hours in the presence of Fe_2O_3-TiO_2 core-shell nanorod arrays. This indicates that the photo-conversion of CO_2 proceeds continuously with the nanorod array catalysts. We also monitored the gas conversion after 24 hours. However, the wide variety of real atmospheric conditions such as sunlight intensity (day and night) and temperature fluctuations prevented quantitative analysis. It is also worthwhile to mention that methanol and methane were also generated in qualitatively observable amounts after 8 hrs exposure. All samples tested shows excellent stability and activity toward MB degradation process and CO_2 conversion even after several uses. No changes in size, shape or morphology of the nanorods were observed as confirmed by the SEM data analysis (data not shown). These results show the benefits of using the Fe_2O_3-TiO_2 core-shell nanostructure for CO_2 conversion applications.

4. Conclusions

In summary, Fe_2O_3-TiO_2 core-shell nanorod arrays active in the UV-Vis region of the spectrum were designed and fabricated using GLAD technique. The optimal annealing temperature is 450-550 °C for the formation of both α-Fe_2O_3 and anatase TiO_2 which work as effective catalysts. The enhanced catalytic efficiency of Fe_2O_3-TiO_2 core-shell samples under visible light illumination was further demonstrated in two applications: photodegradation of MB solution and the photoconversion of CO_2 into fuel gases, which confirms the advantage of the core-shell structures. While these results are promising, several strategies might make the core-shell structure more efficient: hosting an effective reduction catalyst at the exposed TiO_2 surface sites to evolve fuels; hosting effective oxidation catalyst near the reduction catalyst to co-locate intermediate reaction products; and better managing the necessary flux of generated electrons and holes between catalytic sites among others.

Acknowledgement: This work was supported by Department of Energy DOE- Laboratory Directed Research & Development (LDRD) Strategic Initiative Program - DOE under grant number AC819810, UC0066 /PR#8T1764.

References

[1] A.F. Heyduk, Science, 293 (2001) 1639-1641.

[2] S.C. Roy, O.K. Varghese, M. Paulose, C.A. Grimes, ACS Nano 4 (2010) 1259-1278.

[3] S.J.A. Moniz, S.A. Shevlin, D.J. Martin, Z.-X. Guo, J. Tang, Energ. Environ. Sci. 8 (2015) 731-759.

[4] P.V. Kamat, J. Phys. Chem. Lett. 3 (2012) 663-672.

[5] X. Zhang, Y.L. Chen, R.-S. Liu, D.P. Tsai, Rep. Prog. Phys. 76 (2013) 046401.

[6] R. Asahi, T. Morikawa, H. Irie, T. Ohwaki, Chem. Rev. 114 (2014) 9824-9852.

[7] A. Banisharif, A.A. Khodadadi, Y. Mortazavi, A.A. Firooz, J. Beheshtian, S. Agah, S. Menbari, Appl. Catal. B- Environ. 165 (2015) 209-221.

[8] J. Li, N. Wu, Catal. Sci. Tech. 5 (2015) 1360-1384.

[9] A. Fujishima, K. Honda, Nature 238 (1972) 37-38.

[10] S. Pilkenton, S.J. Hwang, D. Raftery, J. Phys. Chem. B 103 (1999) 11152-11160.

[11] S.S. Tan, L. Zou, E. Hu, Catal. Today 115 (2006) 269-273.

[12] O.K. Varghese, M. Paulose, T.J. LaTempa, C.A. Grimes, Nano Lett. 9 (2009) 731-737.

[13] W. Smith, A. Wolcott, R.C. Fitzmorris, J.Z. Zhang, Y. Zhao, J. Mater. Chem. 21 (2011) 10792-10800.

[14] S.I. In, D.D. Vaughn, R.E. Schaak, Angew. Chem. Int. Ed. 51 (2012) 3915-3918.

[15] W. Tu, Y, Zhou, Q. Liu, Z. Tian, J. Gao, X. Chen, H. Zhang, J. Liu, Z. Zou, Adv. Funct. Mater. 22 (2012) 1215-1221.

[16] J. Thomas, K.P. Kumar, S. Mathew, Sci. Adv. Mater. 3 (2011) 59-65.

[17] W. Smith, Y.P. Zhao, J. Phys. Chem. C 112 (2008) 19635-19641.

[18] Z. Luo, H. Jiang, D. Li, L. Hu, W. Geng, P. Wei, P. Ouyang, RSC Adv. 4 (2014) 17797-17804.

[19] G. Liu, Y. Zhao, C. Sun, F. Li, G. Q. Lu, H.-M. Cheng, Angew. Chem. Int. Ed. 47 (2008) 4516-4520.

[20] Z.W. Seh, S. Liu, M. Low, S.-Y. Zhang, Z. Liu, A. Mlayah, M.-Y. Han, Adv. Mater. 24 (2012) 2310-2314.

[21] F. Ye, A. Ohmori, Surf. Coat. Technol. 160 (2002) 62-67.

[22] H. Liu, H.K. Shon, X. Sun, S. Vigneswaran, H. Nan, Appl. Surf. Sci. 257 (2011) 5813-5819.

[23] E.S. Mora, E.G. Barojas, E.R. Rojas, R.S. González, Sol. Energy Mater. Sol. Cells 91 (2007) 1412-1415.

[24] X. Zhang, Y. Xie, H. Chen, J. Guo, A. Meng, C. Li, Appl. Surf. Sci. 317 (2014) 43-48.

[25] H. Liu, L. Gao, J. Am. Ceram. Soc. 89 (2006) 370-373.

[26] Y. Xia, L. Yin, Phys. Chem. Chem. Phys. 15 (2013) 18627-18634.

[27] L. Peng, T. Xie, Y. Lu, H. Fan, D. Wang, Phys. Chem. Chem. Phys. 12 (2010) 8033–8041.

[28] W. Wu, C. Jiang, V.A. L. Roy, Nanoscale 7 (2015) 38-58.

[29] Y. Zhao, D. Ye, G.-C. Wang, T.-M. Lu, Proc. SPIE 5219 (2003) 59-73.

[30] M. M. Hawkeye, M.J. Brett, J. Vac. Sci. Technol. A 25 (2007) 1317-1335.

[31] P. Basnet, Y. Zhao, J. Mater. Chem. A 2 (2014) 911-914.

[32] W. Smith, Y. P. Zhao, Catal. Commun. 10 (2009) 1117-1121.

[33] Y. Zhao, Front. Energy Res. 2 (2014) 38.

[34] J.M. LaForge, G.L. Ingram, M.T. Taschuk, M.J. Brett, Cryst. Growth Des. 12 (2012) 3661-3667.

[35] L.N. Demianets, S.V. Pouchko, R.V. Gaynutdinov, J. Cryst. Growth 259 (2003) 165-178.

[36] P. Basnet, G.K. Larsen, R.P. Jadeja, Y.-C. Hung, Y. Zhao, ACS Appl. Mater. Interfaces 5 (2013) 2085-2095.

[37] M. F. Cansizoglu, R. Engelken, H.W. Seo, T. Karabacak, ACS Nano, 4 (2010) 733-740.

[38] M.F. Al-Kuhaili, M. Saleem, S.M. A. Durrani, J. Alloys Compd. 521 (2012) 178-182.

[39] T. Ohmori, H. Takahashi, H. Mametsuka, E. Suzuki, Phys. Chem. Chem. Phys. 2 (2000) 3519-3522.

[40] M. Mrowetz, W. Balcerski, A.J. Colussi, M.R. Hoffmann, J. Phys. Chem. B 108 (2004) 17269-17273.

[41] D. Chatterjee, S. Rothbart, R.V. Eldik, RSC Adv. 3 (2013) 3606-3610.

[42] K.P. Yu, W.Y. Yu, M.C. Kuo, Y.C. Liou, S.H. Chien, Appl. Catal. B.-Environ. 84 (2008) 112-118.

TABLE I. Parameters of the nanorod array before and after TiO_2 shell deposition.

Sample	Nanorod height: h (nm)	Nanorod top diameter: D_T (nm)	Nanorod separation: d (nm)	Nanorod density: η (μm^{-2})
Fe_2O_3	1220 ± 30	230 ± 50	130 ± 40	10 μm^{-2}
Fe_2O_3- TiO_2	1230 ± 30	240 ± 40	110 ± 60	10 μm^{-2}

TABLE II. Comparison of the photodegradation rates k of different nanorod arrays.

Sample	k (h^{-1}) UV irradiation	k (h^{-1}) Visible light irradiation
Fe_2O_3	Negligible	0.121 ± 0.003
TiO_2	0.245 ± 0.001	0.034 ± 0.001
Fe_2O_3-TiO_2	0.022 ± 0.002	0.151 ± 0.001

Captions

Fig. 1 (a) SEM images of the Fe_2O_3 nanorod array from top view and cross section view. (b) SEM images of the Fe_2O_3-TiO_2 core-shell nanorod array from top view and cross section view.

Fig. 2 (a) HRTEM image of the as-deposited Fe_2O_3-TiO_2 core-shell nanorods. (b)-(d) HRTEM images of the Fe_2O_3-TiO_2 core-shell nanorods annealed at 500 °C.

Fig. 3 (a) EDX spectra of the Fe_2O_3 nanorod array. (b) EDX spectra of the Fe_2O_3 - TiO_2 nanorod array (Note, Si peak is due to substrate).

Fig. 4 XRD patterns of the as-deposited and the annealed Fe_2O_3-TiO_2 core-shell samples.

Fig. 5 UV-Vis spectra: (a) transmittance spectra and (b) absorbance spectra.

Fig. 6 (a) Spectra of the UV light and visible light used for MB degradation. (b) Absorbance of the MB solution with a 450 °C annealed core-shell sample as the photocatalyst, with visible light illumination for 4 hours. (c) Curves of $-\ln(\alpha(t)/\alpha(0))$ versus time from different samples with visible light illumination. (d) Decay rate in dependence of the annealing temperatures of Fe_2O_3-TiO_2 core-shell nanorod array samples, using different light sources.

Fig. 7 (a) H_2 and CO production in the presence of Fe_2O_3-TiO_2 core-shell or TiO_2 nanorod array photocatalysts after 4 hours exposure. (b) H_2 evolution after 16 hours exposure in the presence of TiO_2.

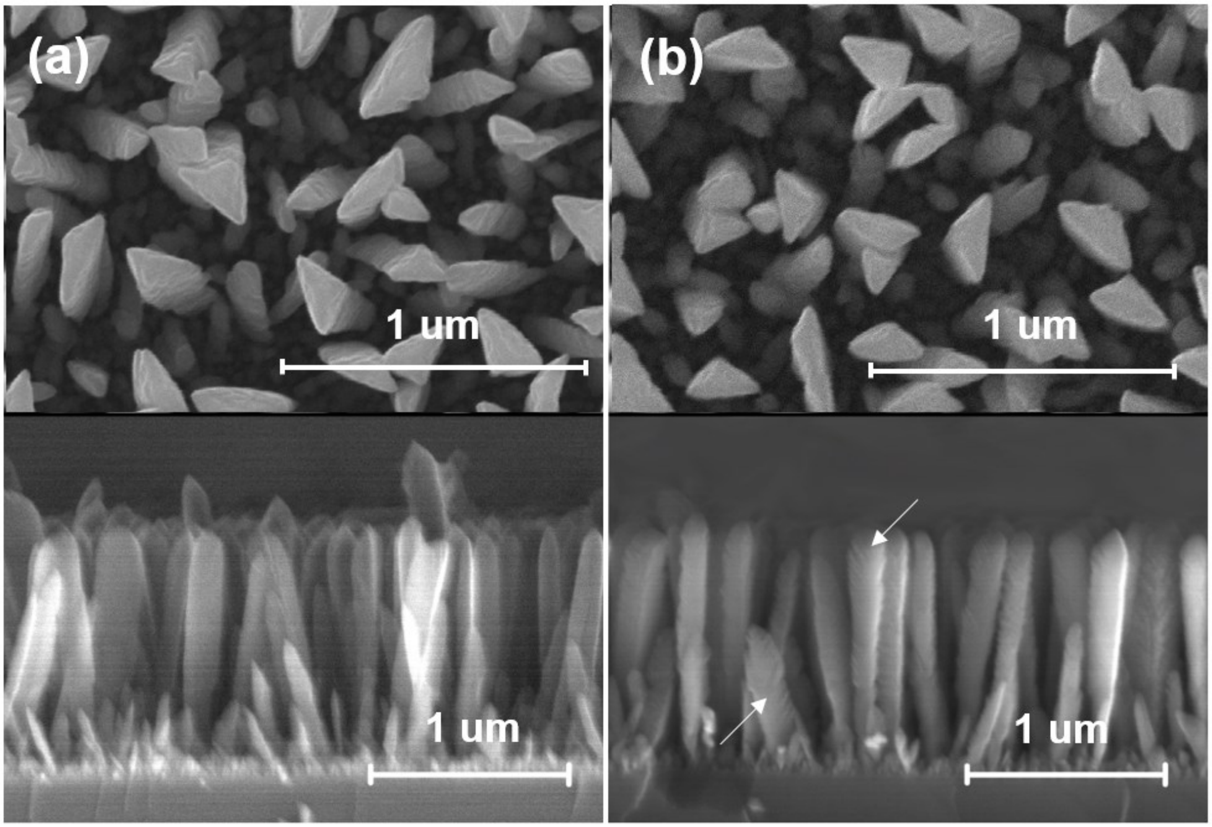

Fig. 1

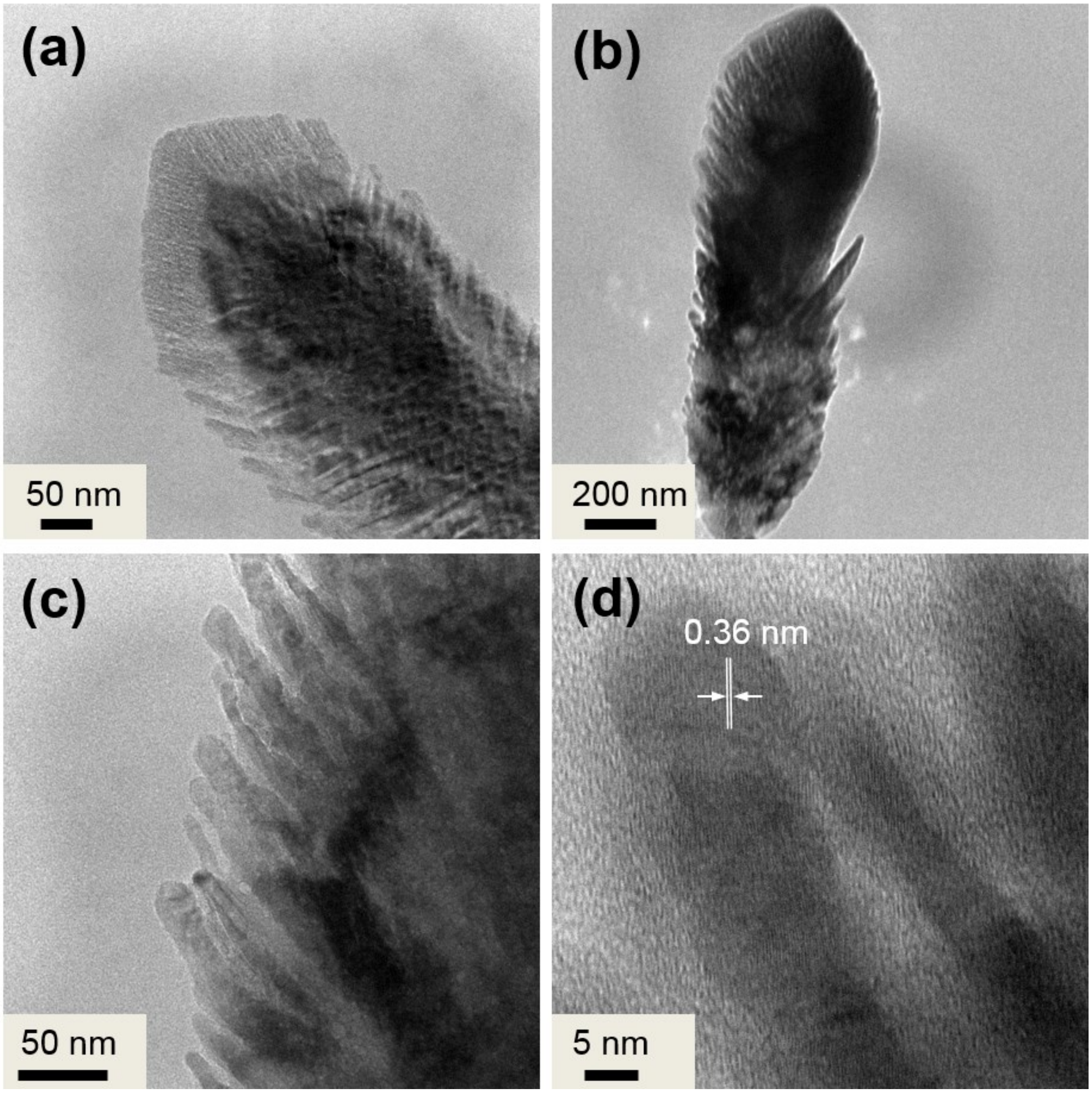

Fig. 2

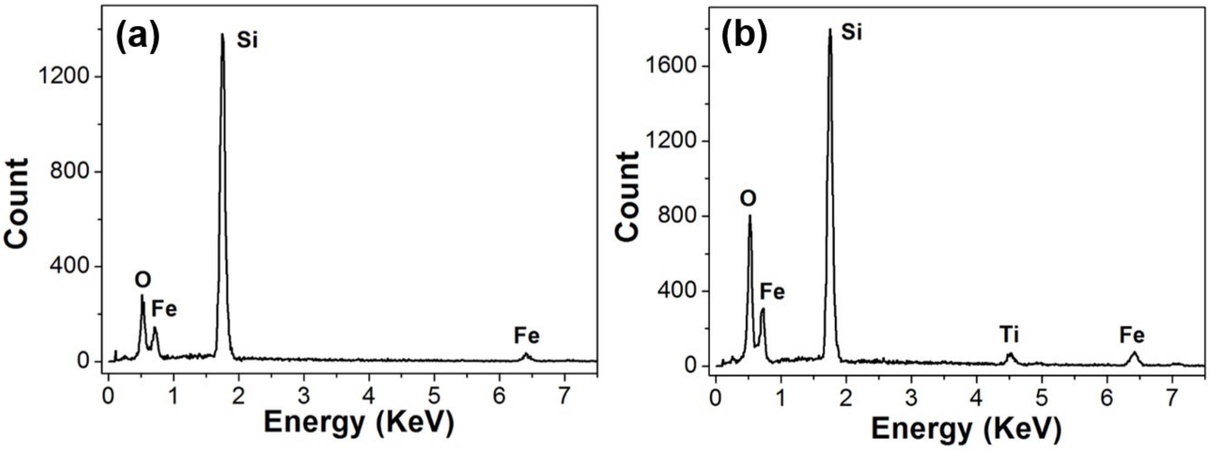
(a)
Si
O
Fe
Fe
Count
0
400
800
1200
Energy (KeV)
0
1
2
3
4
5
6
7
(b)
Si
O
Fe
Ti
Fe
Count
0
400
800
1200
1600
Energy (KeV)
0
1
2
3
4
5
6
7

Fig. 3

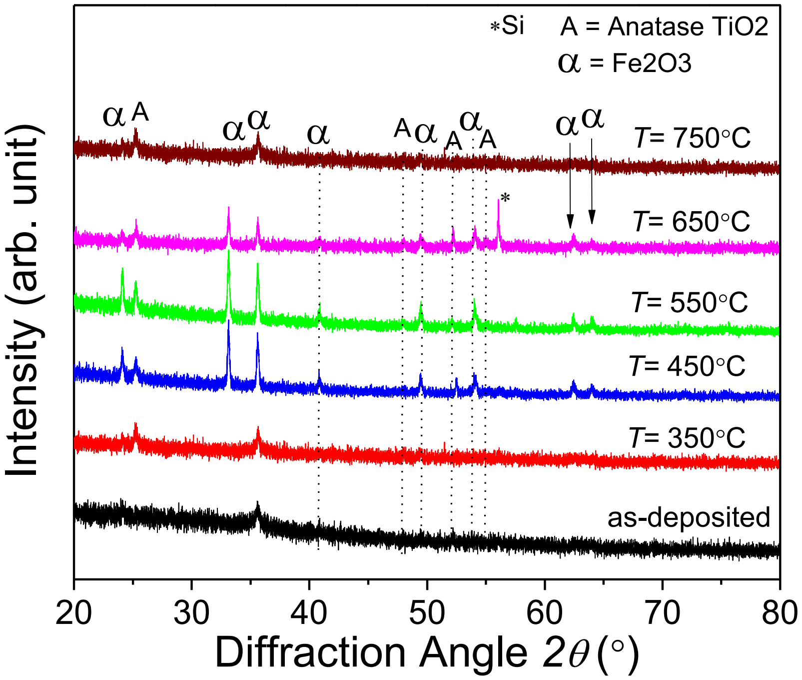

*Si
A = Anatase TiO2
α = Fe2O3
α A
α α
α
A α
A α A
α α
T= 750°C
*
T= 650°C
T= 550°C
T= 450°C
T= 350°C
as-deposited
Intensity (arb. unit)
20
30
40
50
60
70
80
Diffraction Angle 2θ (°)

Fig. 4

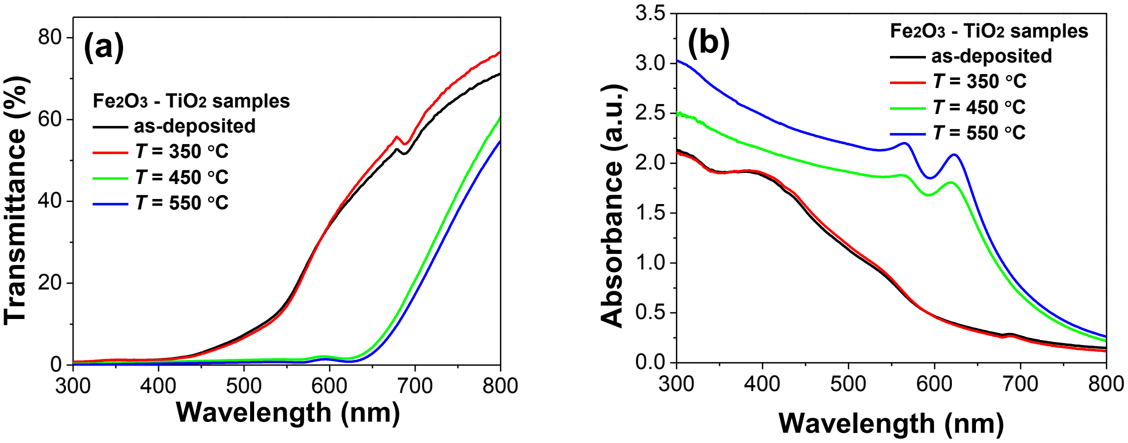
(a)
Transmittance (%)
0
20
40
60
80
Wavelength (nm)
300
400
500
600
700
800
Fe2O3 - TiO2 samples
as-deposited
T = 350 °C
T = 450 °C
T = 550 °C
(b)
Absorbance (a.u.)
0.0
0.5
1.0
1.5
2.0
2.5
3.0
3.5
Wavelength (nm)
300
400
500
600
700
800
Fe2O3 - TiO2 samples
as-deposited
T = 350 °C
T = 450 °C
T = 550 °C

Fig. 5

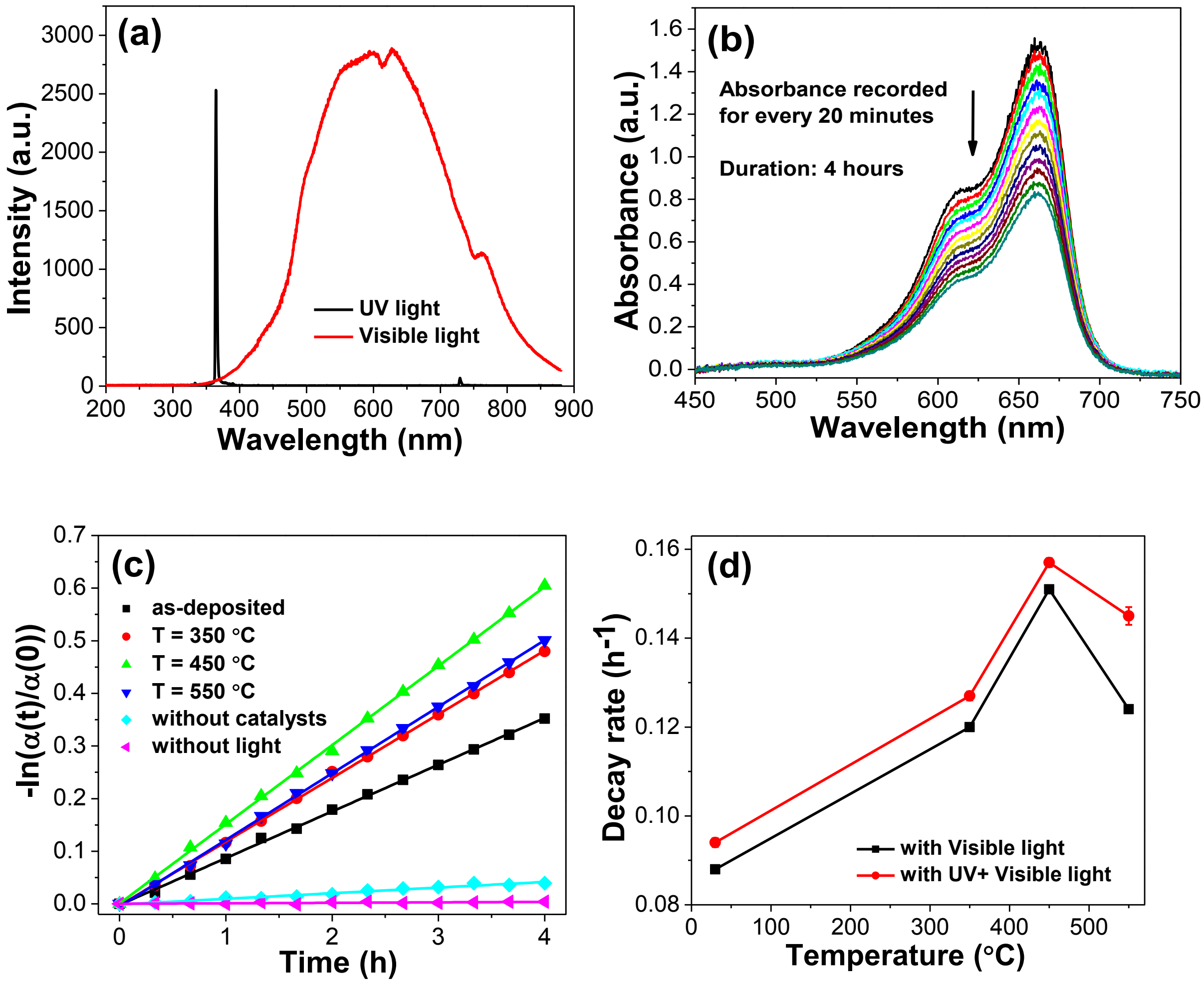
(a)
Intensity (a.u.)
Wavelength (nm)
0
500
1000
1500
2000
2500
3000
200
300
400
500
600
700
800
900
UV light
Visible light
(b)
Absorbance (a.u.)
Wavelength (nm)
Absorbance recorded
for every 20 minutes
Duration: 4 hours
0.0
0.2
0.4
0.6
0.8
1.0
1.2
1.4
1.6
450
500
550
600
650
700
750
(c)
-ln(α(t)/α(0))
Time (h)
0.0
0.1
0.2
0.3
0.4
0.5
0.6
0.7
0
1
2
3
4
as-deposited
T = 350 °C
T = 450 °C
T = 550 °C
without catalysts
without light
(d)
Decay rate (h-1)
Temperature (°C)
0.08
0.10
0.12
0.14
0.16
0
100
200
300
400
500
with Visible light
with UV+ Visible light

Fig. 6

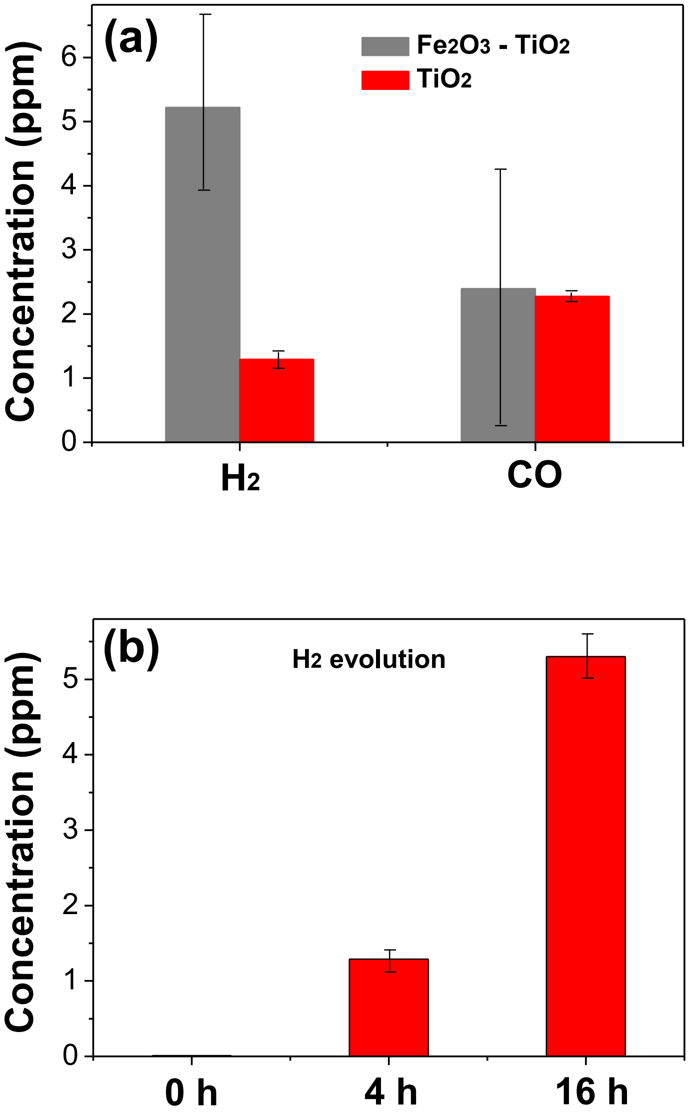
(a)
Fe_2O_3 - TiO_2
TiO_2
Concentration (ppm)
0
1
2
3
4
5
6
H_2
CO
(b)
H_2 evolution
Concentration (ppm)
0
1
2
3
4
5
0 h
4 h
16 h

Fig. 7

Fe_2O_3-TiO_2 Core-Shell Nanorod Arrays for Visible Light Photocatalytic Applications

Kun Yao,[1,2] Pradip Basnet,[2,3] Henry Sessions,[4] George K. Larsen,[4]

Simona E. Hunyadi Murph,[4,5*] and Yiping Zhao[2,3*]

[1] *College of Engineering, University of Georgia, Athens, GA, 30602, USA*

[2] *Nanoscale Science and Engineering Center, University of Georgia, Athens, GA, 30602, USA*

[3] *Department of Physics and Astronomy, University of Georgia, Athens, GA, 30602, USA*

[4] *National Security Directorate, Savannah River National Laboratory, Aiken, SC, USA*

[5] *Chemistry and Physics Department, Georgia Regents University, Augusta, GA, USA*

**Corresponding authors- Email address: Simona.Murph@srnl.doe.gov, Phone: 1-803-646-676,*

Email address: zhaoy@physast.uga.edu, Phone: 1-706-542-7792.

Supplemental Information

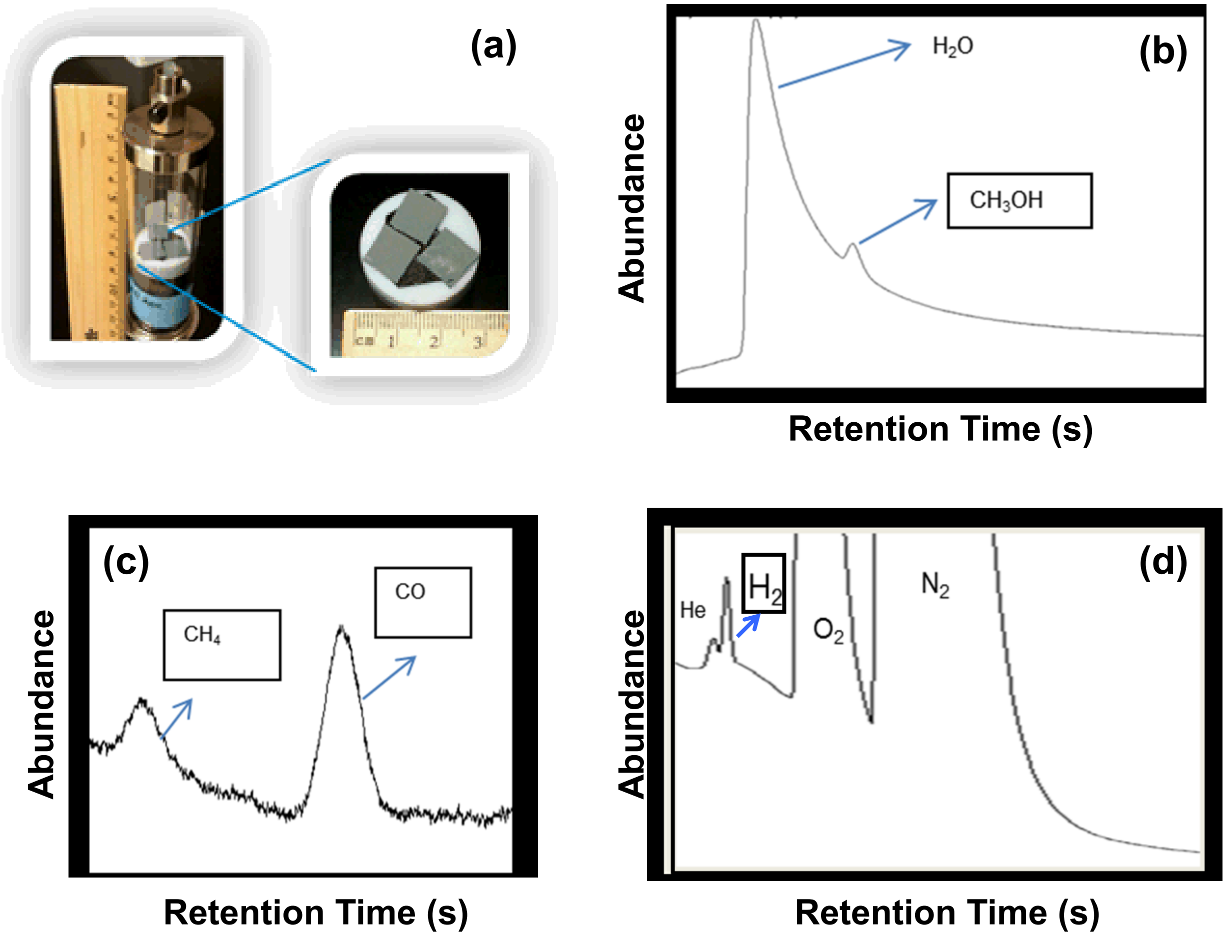

SI Figure 1. (a) Pictures of the syringe-type chamber with the catalysts. (b)-(d) Representative chromatographs collected on a micro-GC showing CO, CH_3OH, CH_4 and H_2 evolution, in the presence of the core-shell nanorod array photocatalysts exposed under ambient light for 4 hours.